

See discussions, stats, and author profiles for this publication at: <https://www.researchgate.net/publication/266393680>

# Structural Changes Observed during the Reversible Hydrogenation of $\text{Mg}(\text{BH}_4)_2$ with Ni-Based Additives

ARTICLE in THE JOURNAL OF PHYSICAL CHEMISTRY C · SEPTEMBER 2014

Impact Factor: 4.77 · DOI: 10.1021/jp5066677

CITATIONS

3

READS

43

8 AUTHORS, INCLUDING:



**Ivan Saldan**

Swedish University of Agricultural Sciences, U...

36 PUBLICATIONS 166 CITATIONS

SEE PROFILE



**Terry D Humphries**

Curtin University

24 PUBLICATIONS 165 CITATIONS

SEE PROFILE



**Olena Zavorotynska**

Institute for Energy Technology - Kjeller, Norway

25 PUBLICATIONS 324 CITATIONS

SEE PROFILE



**Stefano Deledda**

Institute for Energy Technology

54 PUBLICATIONS 487 CITATIONS

SEE PROFILE

# Structural Changes Observed during the Reversible Hydrogenation of $\text{Mg}(\text{BH}_4)_2$ with Ni-Based Additives

I. Saldan,<sup>†,‡</sup> S. Hino,<sup>†</sup> T. D. Humphries,<sup>†</sup> O. Zavorotynska,<sup>†</sup> M. Chong,<sup>§</sup> C. M. Jensen,<sup>§</sup> S. Deledda,<sup>†</sup> and B. C. Hauback<sup>\*,†</sup>

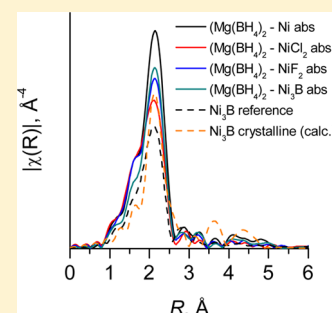
<sup>†</sup>Physics Department, Institute for Energy Technology, P.O. Box 40, NO-2027 Kjeller, Norway

<sup>‡</sup>Department of Physical and Colloid Chemistry, Ivan Franko National University of L'viv, 6 Kyryla and Mefodia Str., UA-79005 L'viv, Ukraine

<sup>§</sup>Department of Chemistry, University of Hawaii, Honolulu, Hawaii 96822, United States

## S Supporting Information

**ABSTRACT:** The decomposition and rehydrogenation of  $\gamma\text{-Mg}(\text{BH}_4)_2$  ball milled together with 2 mol % of Ni-based additives,  $\text{Ni}_{\text{nanor}}$ ,  $\text{NiCl}_2$ ,  $\text{NiF}_2$ , and  $\text{Ni}_3\text{B}$ , has been investigated during one hydrogen desorption–absorption cycle. Under the applied ball-milling conditions, no mechanochemical reactions between  $\gamma\text{-Mg}(\text{BH}_4)_2$  and  $\text{Ni}_{\text{add}}$  were observed. Hydrogen desorption carried out at temperatures of 220–264 °C resulted for all samples in partial decomposition of  $\text{Mg}(\text{BH}_4)_2$  and formation of amorphous phases, as seen by powder X-ray diffraction (PXD). PXD analysis after rehydrogenation at temperatures of 210–262 °C and at pressures between 100 and 155 bar revealed increased fractions of crystalline  $\beta\text{-Mg}(\text{BH}_4)_2$ , indicating a partial reversibility of the composite powders. The highest amount of  $[\text{BH}_4]^-$  is formed in the composite containing  $\text{Ni}_3\text{B}$ . Analysis by X-ray absorption spectroscopy performed after ball milling, after desorption, and after absorption shows that the  $\text{Ni}_3\text{B}$  additive remains unaffected, whereas  $\text{NiCl}_2$  and  $\text{NiF}_2$  additives react with  $\text{Mg}(\text{BH}_4)_2$  during the hydrogen desorption–absorption and form compounds with a local structure very similar to that of amorphous  $\text{Ni}_3\text{B}$ . Multinuclear NMR spectroscopy confirms the partial reversibility of the system as well as the formation of  $[\text{B}_{10}\text{H}_{10}]^{2-}$  during hydrogen absorption. The presence of  $[\text{B}_n\text{H}_n]^{2-}$  ( $n = 10, 12$ ) was also detected by infrared (IR) spectroscopy of the dehydrogenated and rehydrogenated samples. The IR measurements give no clear indication that ions containing B–H–B bridged hydrogen groups were formed during the H-sorption cycle.



## 1. INTRODUCTION

Magnesium borohydride,  $\text{Mg}(\text{BH}_4)_2$ , is one of the most promising hydrogen storage materials due to its theoretical hydrogen capacity of 14.9 wt %.<sup>1</sup> However, its application is hindered by poor kinetics and lack of reversibility. The decomposition of  $\text{Mg}(\text{BH}_4)_2$  occurs via several steps, and the resulting products and intermediates vary depending on the experimental conditions.<sup>2–6</sup> The main hydrogen release in pure  $\text{Mg}(\text{BH}_4)_2$  occurs between 270 and 320 °C. In this temperature region, a variety of intermediate amorphous magnesium polyboranes are formed before decomposition to  $\text{MgH}_2$  and amorphous boron. The formation of stable higher polyborane intermediates, such as  $\text{MgB}_{12}\text{H}_{12}$ ,<sup>7,8</sup> has been proposed to be the main factor hindering reversible hydrogenation of  $\text{Mg}(\text{BH}_4)_2$ . The icosahedral framework in  $\text{MgB}_{12}\text{H}_{12}$  and that of bulk boron is a reason for the thermal stability of the polyboranes.<sup>9</sup> On the other hand, the synthesis of  $\text{Mg}(\text{BH}_4)_2$  from lower polyboranes (e.g.,  $\text{Mg}(\text{B}_3\text{H}_8)_2$ ) has been demonstrated at a relatively low hydrogen pressure and temperature ( $\sim 120$  bar of  $\text{H}_2$  and 250 °C).<sup>10</sup> Decomposition of  $\text{Mg}(\text{BH}_4)_2$  to  $\text{Mg}(\text{B}_3\text{H}_8)_2$  is reported to be reversible with theoretical hydrogen storage capacity of 2.5 wt %.<sup>10</sup>

An additive that changes the reaction pathway and thus inhibits the formation of stable higher polyboranes is one of the possibilities that could improve the reversibility of H-sorption in  $\text{Mg}(\text{BH}_4)_2$ . Development of effective additives to improve the hydrogen desorption–absorption is therefore crucial before use as a hydrogen storage material.

Transition metals have the ability to bond to hydrogen in a variety of stoichiometries. This promotes fast dissociation of molecular hydrogen into atomic hydrogen or its recombination back to hydrogen molecules.<sup>11</sup> Nickel additives have recently gained interest for their catalytic activity toward the reversible hydrogenation of complex hydrides. The valence of Ni in the  $\text{NiCl}_2$ -activated  $\text{LiBH}_4 + 0.5\text{MgH}_2$  and  $\text{Li}_3\text{BN}_2\text{H}_8$  hydrogen storage materials is close to zero and invariant during hydrogen cycling when analyzed by X-ray absorption spectroscopy (XAS).<sup>12,13</sup> Moreover, Ni-doped  $\text{LiBH}_4 + 0.5\text{MgH}_2$  initially forms amorphous  $\text{Ni}_3\text{B}$ , which is partially converted to amorphous  $\text{Mg}_2\text{NiH}_x$  upon hydrogen absorption. Surface calculations performed using density functional theory suggest

Received: July 3, 2014

Revised: August 28, 2014

Published: September 11, 2014

that the lowest kinetic barrier for  $\text{H}_2$  chemisorption occurs on the  $\text{Ni}_3\text{B}$  (100) surface.<sup>12</sup> The order of catalytic activity of Ni additives toward the hydrogenation of benzene was established to be as follows: nanocrystalline Ni > nanoamorphous Ni–B alloy > crystalline Ni  $\approx$  crystalline  $\text{Ni}_3\text{B}$ .<sup>14</sup> Ni-based additives, such as Ni nanoparticles,  $\text{Ni}_3\text{B}$ ,  $\text{NiCl}_2$ ,  $\text{NiF}_2$ , and Ni (65 wt % on  $\text{Si}/\text{Al}_2\text{O}_3$ ), have also been demonstrated to decrease the temperature of hydrogen desorption in  $\text{NaBH}_4$  by at least 60 °C.<sup>15</sup>

In the present work, four different Ni-based additives,  $\text{Ni}_{\text{nano}}$ ,  $\text{NiCl}_2$ ,  $\text{NiF}_2$ , and  $\text{Ni}_3\text{B}$ , have been investigated with respect to their effect on the reversible  $\text{Mg}(\text{BH}_4)_2$  decomposition. Qualitative analysis of the additives during hydrogen desorption–absorption were performed by X-ray absorption near edge spectroscopy/extended X-ray absorption fine structure (XANES/EXAFS) as a “finger print” method, and their Fourier transforms were used to determine the interatomic distances between Ni and other neighboring atoms. The borane species present after desorption–absorption were characterized by  $^{11}\text{B}$  and  $^1\text{H}$  NMR and infrared (IR) spectroscopy.

## 2. EXPERIMENTAL METHODS

Commercial  $\gamma\text{-Mg}(\text{BH}_4)_2$  ( $\geq 95\%$ , Sigma-Aldrich) was used to prepare  $\text{Mg}(\text{BH}_4)_2\text{-Ni}_{\text{add}}$  ( $\text{Ni}_{\text{add}} = \text{Ni}_{\text{nano}}$  (30 nm, Nano-structured & Amorphous, Inc.),  $\text{NiCl}_2$  (99.99%, Sigma-Aldrich),  $\text{NiF}_2$  (Sigma-Aldrich), and  $\text{Ni}_3\text{B}$  (synthesized in-house)) composites with 2 mol % of additives by ball-milling. Synthesis of  $\text{Ni}_3\text{B}$  was carried out as described by Kapfenberger et al.<sup>16</sup> An aqueous 2 M solution of  $\text{NaBH}_4$  was added dropwise to an ice-cooled 0.27 M aqueous solution of  $\text{NiCl}_2$  over 45 min, during which effervescence and formation of a black precipitate was observed. The precipitate was then collected by filtration and washed with water, followed by washing with EtOH. The amorphous solid was allowed to dry in air overnight, giving a yield of 62%. The identity of the amorphous powder was confirmed by powder X-ray diffraction (PXD) after annealing a small quantity at 350 °C for 1.3 h. PXD analysis indicated the presence of  $\text{Ni}_3\text{B}$  as the major phase (ICDD PDF 00-001-1260) with some metallic Ni. The amorphous powder was used as the additive.

Milling was conducted in a Fritsch Pulverisette 7 planetary mill with tempered steel vials (26 mL volume) and balls (10 mm diameter) in Ar atmosphere. A ball-to-powder mass ratio of 40:1 was employed, with a milling time of 1 h at a speed of 300 rpm. All powder manipulations were carried out in MBraun Unilab glove boxes filled with purified argon (<1 ppm of  $\text{O}_2/\text{H}_2\text{O}$ ).

Hydrogen sorption measurements were carried out in an in-house manufactured Sieverts type apparatus.<sup>17</sup> All  $\text{Mg}(\text{BH}_4)_2\text{-Ni}_{\text{add}}$  composites were dehydrogenated under static vacuum ( $\sim 10^{-5}$  mbar) and rehydrogenated under 100–155 bar of  $\text{H}_2$ . The hydrogenation reaction conditions of all composites are summarized in Table 1.

PXD patterns were collected in Debye–Scherrer geometry using Cu  $K\alpha$  radiation ( $\lambda = 1.5418 \text{ \AA}$ ) using a Bruker AXS D8 Advance Diffractometer equipped with a Göbbel mirror and a LynxEye 1D strip detector. The diffraction patterns were obtained using rotating boron glass capillaries, filled and sealed under Ar atmosphere. Small amounts of pure Si (ABCR, APS 1–5  $\mu\text{m}$ , 99.999%) were added as an internal standard to enable Bragg peak position correction. Data acquisition was

**Table 1. Experimental Conditions and Hydrogen Storage Capacities during Desorption and Hydrogen Reabsorption for  $\text{Mg}(\text{BH}_4)_2\text{-Ni}_{\text{add}}$  ( $\text{Ni}_{\text{add}} = \text{Ni}_{\text{nano}}$ ,  $\text{NiCl}_2$ ,  $\text{NiF}_2$ ,  $\text{Ni}_3\text{B}$ ) Composites**

	$\text{Mg}(\text{BH}_4)_2\text{-Ni}_{\text{add}}$ composite			
	$\text{Ni}_{\text{nano}}$	$\text{NiCl}_2$	$\text{NiF}_2$	$\text{Ni}_3\text{B}$
desorption temperature (°C)	256	258	264	220
desorption time (h)	60	10	30	15
absorption temperature (°C)	251	253	262	210
absorption pressure (bar)	140	140	100	155
absorption time (h)	20	15	10	48
$\text{H}_2$ desorbed (wt %)	2.7	2.7	6.5	2.7
$\text{H}_2$ absorbed (wt %)	1.3	1.2	2.0	1.0

restricted to  $2\theta = 5\text{--}60^\circ$ , with  $\Delta 2\theta = 0.02^\circ$  and 2 s/step scanning rates.

EXAFS spectra were collected at beamline I811 at MaxLab (Lund, Sweden) in the energy range 8200–9000 eV of Ni K-edge (8331.4 eV) at room temperature.<sup>18</sup> Boron nitride (BN)-2 mol %  $\text{Ni}_{\text{nano}}$ ,  $\text{NiCl}_2$ ,  $\text{NiF}_2$ , and  $\text{Ni}_3\text{B}$  mixtures were measured for reference. Finely ground powders were pressed into pellets, which were mounted into special aluminum plates. To avoid oxidation, the plates were covered by polyimide film adhered by high-vacuum grease. EXAFS data were measured in fluorescence mode, six times for each sample (where four quick scans were used for sample adjustments). Two step scans were measured in pre-edge and edge regions with counting time of 0.5 s and in EXAFS region  $\sim 20$  s per point. All presented data analyses were performed using ATHENA and ARTEMIS software.<sup>19</sup>

$^1\text{H}$  and  $^{11}\text{B}$  NMR solution spectroscopy was carried out on a Varian Unity Innova 500 MHz spectrometer with  $^{11}\text{B}$  chemical shifts referenced to  $\text{BF}_3\cdot\text{OEt}_2$  ( $\delta = 0$  ppm) at 20 °C. All  $^1\text{H}$  were referenced to the  $\text{D}_2\text{O}$  peak at 4.79 ppm. Deuterium oxide was chosen as the solvent for the NMR studies because it allowed for the most complete dissolution of the sample powders.<sup>10</sup> As a consequence, however, any boranes possessing open cage structures, such as *nido* or *arachno* boranes tend to hydrolyze, usually appearing somewhat downfield of 0 ppm.<sup>20–22</sup>

Attenuated total reflection Fourier transformed infrared (ATR FT-IR) spectra were measured on a Bruker Alpha-Platinum infrared spectrometer upon a diamond crystal. The spectra were obtained in the range of 4000–400  $\text{cm}^{-1}$ , with a resolution of 2  $\text{cm}^{-1}$ , with 32 scans averaged for each spectrum and the background. The samples were measured without any dilution. All IR measurements were conducted in an argon-filled glovebox.

## 3. RESULTS AND DISCUSSION

**3.1. Hydrogen Desorption–Absorption and PXD Analysis.** Each of the milled  $\text{Mg}(\text{BH}_4)_2\text{-2 mol \% Ni}_{\text{add}}$  composites were dehydrogenated in the Sieverts type apparatus at temperatures between 220 and 264 °C. This temperature range was chosen to promote partial decomposition and, in particular, the formation of  $\text{Mg}(\text{B}_3\text{H}_8)_2$  rather than the thermodynamically stable polyboranes, e.g.,  $\text{MgB}_{12}\text{H}_{12}$ .<sup>7,8</sup> These conditions are close to those utilized in a previous study in which  $\text{Mg}(\text{B}_3\text{H}_8)_2$  was demonstrated to be reversibly hydrogenated to  $\text{Mg}(\text{BH}_4)_2$ .<sup>10</sup> Hydrogen absorption was then performed on the dehydrogenated powders in order to reform

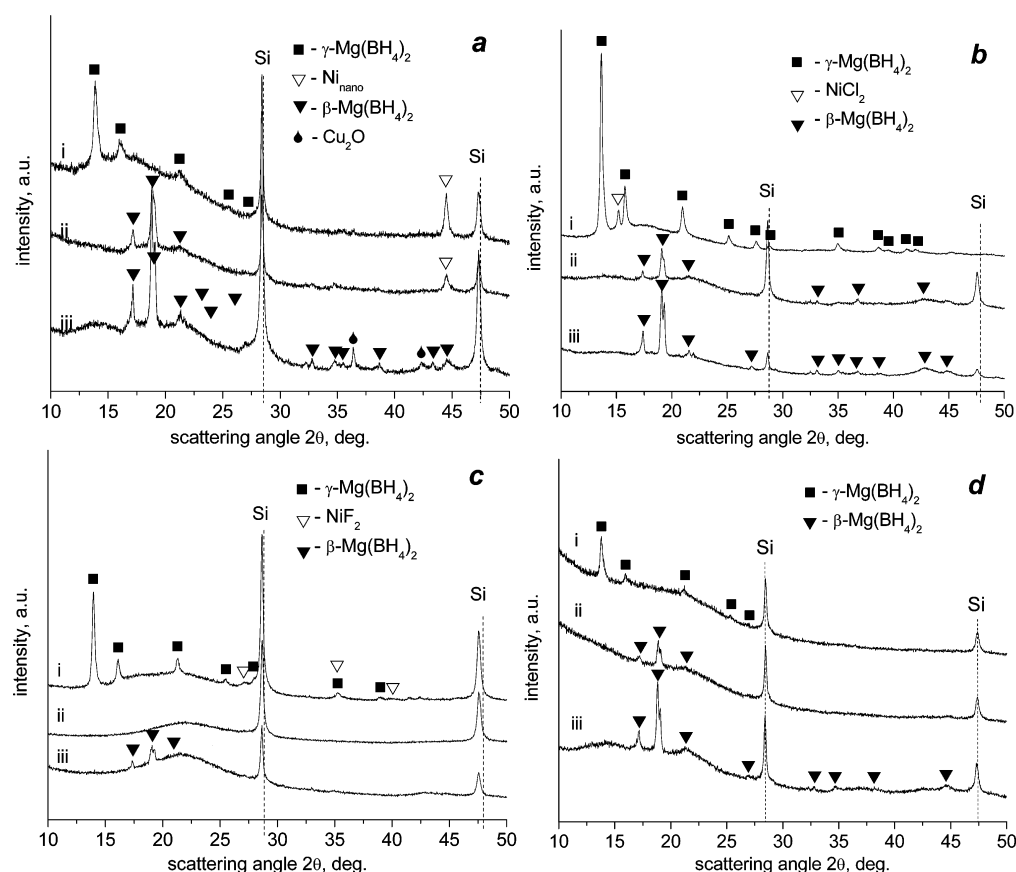


**Figure 1.** PXD patterns for  $\text{Mg}(\text{BH}_4)_2\text{-Ni}_{\text{add}}$  ( $\text{Ni}_{\text{add}}$  = (a)  $\text{Ni}_{\text{nano}}$ ; (b)  $\text{NiCl}_2$ ; (c)  $\text{NiF}_2$ ; (d)  $\text{Ni}_3\text{B}$ ) composites (i) as milled, (ii) after hydrogen desorption, and (iii) after hydrogen absorption. Additional impurity of  $\text{Cu}_2\text{O}$  detected for  $\text{Mg}(\text{BH}_4)_2\text{-Ni}_{\text{nano}}$  composites in panel a after absorption is due to contamination during preparation of the PXD specimen.

$\text{Mg}(\text{BH}_4)_2$ . The experimental conditions along with quantitative results for desorption–absorption are given in Table 1.

The results of the desorption experiments on the composites containing  $\text{Ni}_{\text{nano}}$ ,  $\text{NiCl}_2$ , and  $\text{Ni}_3\text{B}$  indicate that the hydrogen content (approximately  $\sim 2.5$  wt % of  $\text{H}_2$ ) corresponds to the theoretical value expected for the formation of  $\text{Mg}(\text{B}_3\text{H}_8)_2$ . However, the time required for hydrogen desorption (up to 60 h) is significantly reduced compared to 5 weeks at  $200^\circ\text{C}$  reported for pure  $\text{Mg}(\text{BH}_4)_2$ .<sup>10</sup> This suggests an apparent effectiveness of Ni-based additives in promoting hydrogen desorption in  $\text{Mg}(\text{BH}_4)_2$ , although the higher operating temperatures used in our work during desorption also play a beneficial role for improving the desorption kinetics. The high desorption value obtained for  $\text{Mg}(\text{BH}_4)_2\text{-NiF}_2$  ( $\sim 6.5$  wt % of  $\text{H}_2$ ) might be due to the effect of a slightly higher temperature. After desorption, each sample absorbed 1–2 wt %  $\text{H}_2$ . The reasons for this discrepancy can be ascribed to several interplaying factors: (1) the gas desorbed was not pure hydrogen but consisted also of, for instance,  $\text{B}_2\text{H}_6$ ; (2) some irreversible phases were formed during desorption; and (3) the absorption pressure was not high enough to completely reform  $\text{Mg}(\text{BH}_4)_2$ .

PXD patterns of the  $\text{Mg}(\text{BH}_4)_2\text{-Ni}_{\text{add}}$  composites, in the as-milled, desorbed and absorbed state, were collected for phase identification. Although moderate milling conditions were employed, slight amorphization of  $\gamma\text{-Mg}(\text{BH}_4)_2$  takes place during milling (see PXD for as-milled samples, patterns (i) in Figure 1), as previously reported by Li et al.<sup>23</sup> This may be because the ball milling can easily induce the collapse of the

highly porous structure of  $\gamma\text{-Mg}(\text{BH}_4)_2$ .<sup>24</sup> The remaining fraction of crystalline  $\gamma\text{-Mg}(\text{BH}_4)_2$  undergoes an irreversible phase transformation via the  $\epsilon$  polymorph to  $\beta\text{-Mg}(\text{BH}_4)_2$  upon heating to  $200^\circ\text{C}$ .<sup>25</sup> This is in agreement with our PXD results: in all samples desorption is not complete, and the remaining fraction of  $\text{Mg}(\text{BH}_4)_2$  is the  $\beta$ -modification (see PXD after desorption, patterns (ii) in Figure 1). After absorption of  $\text{H}_2$ , all  $\text{Mg}(\text{BH}_4)_2\text{-Ni}_{\text{add}}$  composites exhibit an increased relative intensity of the  $\beta\text{-Mg}(\text{BH}_4)_2$  peaks when compared with the PXD patterns after desorption. This indicates that during rehydrogenation, magnesium borohydride partially reforms from the desorbed samples.

While PXD analysis confirms slight amorphization of  $\gamma\text{-Mg}(\text{BH}_4)_2$  in all as-milled  $\text{Mg}(\text{BH}_4)_2\text{-Ni}_{\text{add}}$  composites, it does not provide much information about the nature of the Ni additives.  $\text{NiCl}_2$  and  $\text{Ni}_{\text{nano}}$  can still be detected after milling; however, the Bragg peaks for  $\text{NiF}_2$  are obscured by those for  $\text{Mg}(\text{BH}_4)_2$ , rendering the identification of the additive problematic. Furthermore, because amorphous nickel boride was used for the composite preparation, this additive is not detectable by PXD. All Ni additives (with the exception of  $\text{Ni}_{\text{nano}}$ ) were not detected by PXD after the hydrogen desorption–absorption cycle. Therefore, X-ray absorption spectroscopy was used as a suitable technique for monitoring the local chemical structure of the Ni additives.

### 3.2. X-ray Absorption Spectroscopy at the Ni K-Edge.

XAS at the Ni K-edge, measured in the range of 8200–9000 eV, was used to determine the local structure around the Ni atoms. EXAFS represents the fractional change in the

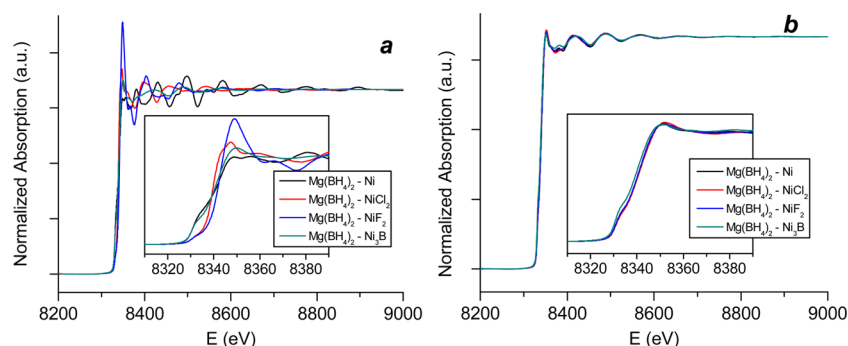


**Figure 2.** Normalized X-ray absorption spectra of  $\text{Mg}(\text{BH}_4)_2\text{-Ni}_{\text{add}}$  ( $\text{Ni}_{\text{add}} = \text{Ni}_{\text{nano}}, \text{NiCl}_2, \text{NiF}_2, \text{Ni}_3\text{B}$ ) composites (a) after milling and (b) after hydrogen desorption–absorption.

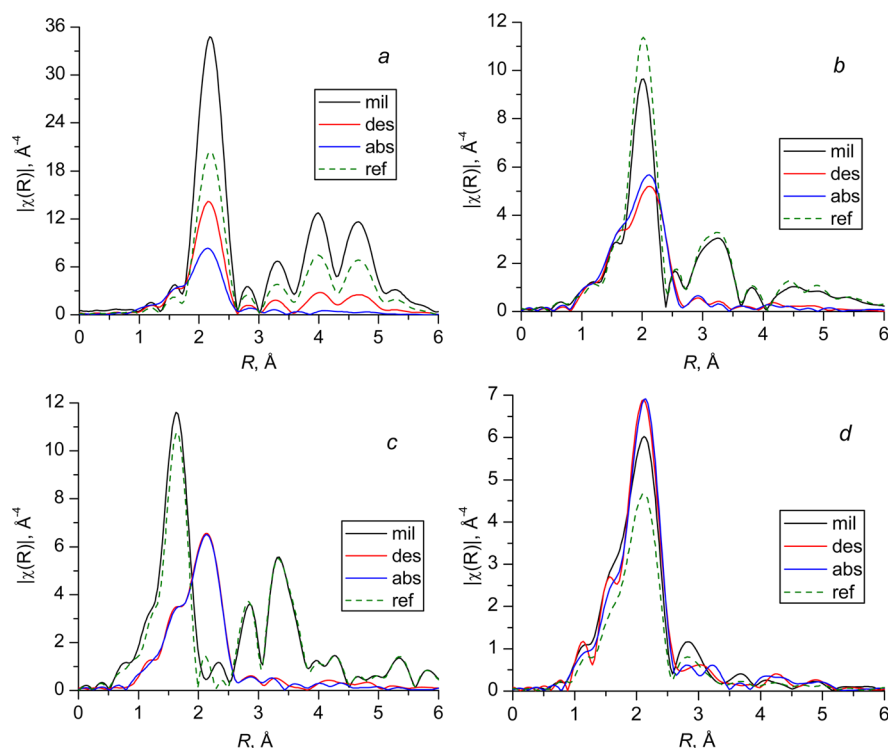


**Figure 3.** Fourier transform of  $k^3$ -weighted  $\chi(k)$  function for  $\text{Mg}(\text{BH}_4)_2\text{-Ni}_{\text{add}}$  ( $\text{Ni}_{\text{add}} =$  (a)  $\text{Ni}_{\text{nano}}$ , (b)  $\text{NiCl}_2$ , (c)  $\text{NiF}_2$ , (d)  $\text{Ni}_3\text{B}$ ) composites in the as-milled state (mil), after the first hydrogen desorption (des), and following absorption (abs) together with corresponding Ni additive as reference (ref).

absorption coefficient induced by neighboring atoms and contains only structural information. Figure 2 illustrates the normalized absorption spectra of the  $\text{Mg}(\text{BH}_4)_2\text{-Ni}_{\text{add}}$  composites (as-milled and after hydrogen desorption–absorption).

The individual spectral profiles of the as-milled samples in Figure 2a are noticeably different, indicating that each additive has dissimilar neighboring atoms around the respective Ni atoms. Each profile is basically identical to that of each reference material (shown in the Supporting Information), suggesting that the structure of the various Ni-additives were preserved after milling. However, after hydrogen desorption–absorption (Figure 2b), the EXAFS spectra are nearly indistinguishable. The two insets in Figure 2 show the XANES data in the energy region of 8200–8390 eV. The  $\text{Mg}(\text{BH}_4)_2$  composites containing  $\text{NiCl}_2$  and  $\text{NiF}_2$  show a small shift of the Ni-edge to higher energies compared to those of  $\text{Ni}_{\text{nano}}$  and  $\text{Ni}_3\text{B}$ , indicating that the Ni exists in a higher

oxidation state (inset in Figure 2a). When the metal center possesses a higher oxidation state, the attraction between the electrons and nucleus increases as the removal of the valence electrons reduces the shielding of the core electrons from the nucleus. For the rehydrogenated  $\text{Mg}(\text{BH}_4)_2\text{-Ni}_{\text{add}}$  composites, all of the XANES spectra (inset in Figure 2b) are almost identical, indicating that the Ni atoms exist in the same oxidation state. In light of these facts, it is proposed that during hydrogen desorption–absorption, the Ni additives react to form a new Ni compound that might be responsible for the enhanced desorption activity of  $\text{Mg}(\text{BH}_4)_2$ .

Fourier transform (FT) of the XAFS data is useful for separating XAFS frequency functions and converting them to corresponding peaks in real space, with the aim of extracting the interatomic distances ( $R$ ) between the absorber and backscattering coordination shell. FT of the  $k^3$ -weighted  $\chi(k)$  function for the milled, dehydrogenated, and rehydrogenated  $\text{Mg}(\text{BH}_4)_2\text{-Ni}_{\text{add}}$  composites is shown in Figure 3. The FTs for



each as-milled composite are very similar to those of the respective Ni-containing references. This suggests that the atomic distribution around the Ni atom is practically unchanged after milling and that the milling process does not result in chemical reaction between the  $\text{Mg}(\text{BH}_4)_2$  and the additives.

Analysis of the Ni nanopowder composite samples (Figure 3a) indicates that the main peak at 2.2 Å is from the Ni nearest neighbor and peaks in the range of 3–5 Å correspond to second, third, and fourth nearest shells. The Ni–Ni distances measured in the milled and desorbed  $\text{Mg}(\text{BH}_4)_2$ – $\text{Ni}_{\text{nano}}$  composites are very similar to those of the Ni nanopowder reference sample in Figure 3a. This suggests an almost identical Ni local structure and confirms the presence of metallic Ni as identified by PXD. However, the intensities of peaks above 3 Å are reduced compared to the first peak in the desorbed sample, indicating a lower degree of long-range order. After hydrogen absorption, the intensity of the main peak at ~2.1 Å has decreased and peaks above 3.5 Å are barely visible. This is indicative of a higher degree of disorder in the medium- and long-range around the central Ni atom.

The spectra of the  $\text{Mg}(\text{BH}_4)_2$ – $\text{NiCl}_2$  and  $\text{Mg}(\text{BH}_4)_2$ – $\text{NiF}_2$  composites (Figure 3b,c) show an alternative trend. For these Ni additives, the first coordination shell around the central Ni atom consists of lighter atoms (Cl or F). After hydrogen desorption, the XANES and EXAFS profiles of these samples are dramatically altered from their initial state, suggesting the local environment of the Ni atom is chemically and structurally different. At the same time it is similar to that observed for  $\text{Ni}_3\text{B}$ . Following hydrogen absorption, these configurations remain, suggesting that the central Ni atom undergoes no further reaction during the hydrogenation process.

The FTs for the  $\text{Mg}(\text{BH}_4)_2$ – $\text{Ni}_3\text{B}$  composites after milling, desorption, and absorption (Figure 3d) show similar patterns. The shoulder at 1.6 Å corresponds to the nearest B shell, and the main peak at ~2.1 Å corresponds to the nearest Ni shell.<sup>26</sup> Absence of major peaks above 3 Å implies medium- and long-range disorder in the local environment of Ni. This is due to the amorphous nature of the as-prepared  $\text{Ni}_3\text{B}$ . The lack of difference in the long-range order suggests that the crystallization of amorphous  $\text{NiB}_3$ , which is possible at the temperatures used for absorption, has not occurred.<sup>26–30</sup> This is confirmed by PXD analysis (see Figure 1d).

Figure 4 compares the FTs for all rehydrogenated  $\text{Mg}(\text{BH}_4)_2$ – $\text{Ni}_{\text{add}}$  composites together with the FT for the

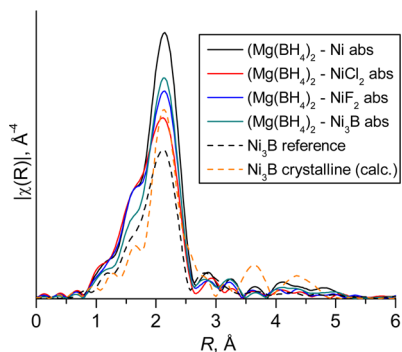


**Figure 4.** Fourier transform of  $k^3$ -weighted  $\chi(k)$  function of  $\text{Mg}(\text{BH}_4)_2$ – $\text{Ni}_{\text{add}}$  ( $\text{Ni}_{\text{add}} = \text{Ni}_{\text{nano}}, \text{NiCl}_2, \text{NiF}_2, \text{Ni}_3\text{B}$ ) composites after hydrogen desorption–absorption; synthesized  $\text{Ni}_3\text{B}$  as reference and calculated crystalline  $\text{Ni}_3\text{B}$ .

synthesized amorphous  $\text{Ni}_3\text{B}$  reference. The FT for crystalline  $\text{Ni}_3\text{B}$  calculated using crystallographic data is also included in Figure 4. It can be noted that for all rehydrogenated  $\text{Mg}(\text{BH}_4)_2$ – $\text{Ni}_{\text{add}}$  composites, XANES and EXAFS profiles are almost identical and are similar to those of amorphous  $\text{Ni}_3\text{B}$ . This suggests that in all composites, a Ni species with a local structure similar to that of  $\text{Ni}_3\text{B}$  forms after hydrogen desorption–absorption. These conclusions are not surprising, as a recent cycling study of  $\text{NaBH}_4$  with similar Ni additives yielded identical observations by PXD.<sup>15</sup> It is reasonable that during the decomposition of  $\text{Mg}(\text{BH}_4)_2$  composites, chemical reaction between the Ni additives and the intermediate B-containing species prevails to form a thermodynamically stable  $\text{Ni}_x\text{B}_y$  species. In this work,  $\text{Ni}_3\text{B}$  appears to be the most stable  $\text{Ni}_x\text{B}_y$  species as no further reaction occurs during subsequent hydrogenation.

**3.3.  $^1\text{H}$  and  $^{11}\text{B}$  NMR Spectroscopy Studies.** In an effort to understand the phases that are formed during desorption and absorption,  $^1\text{H}$  and  $^{11}\text{B}$  NMR spectroscopy studies were performed in  $\text{D}_2\text{O}$  on each of the  $\text{Mg}(\text{BH}_4)_2$ – $\text{Ni}_{\text{add}}$  composites after H-sorption and on pure  $\gamma$ - $\text{Mg}(\text{BH}_4)_2$  as reference. NMR spectroscopy enables the identification of phases that, if amorphous, cannot be detected by PXD. This is particularly helpful for the study of borane-containing species. The  $^1\text{H}$  NMR spectra of  $\text{Mg}(\text{BH}_4)_2$ – $\text{Ni}_{\text{add}}$  composites after desorption and absorption are presented in Figure 5. A broad multiplet

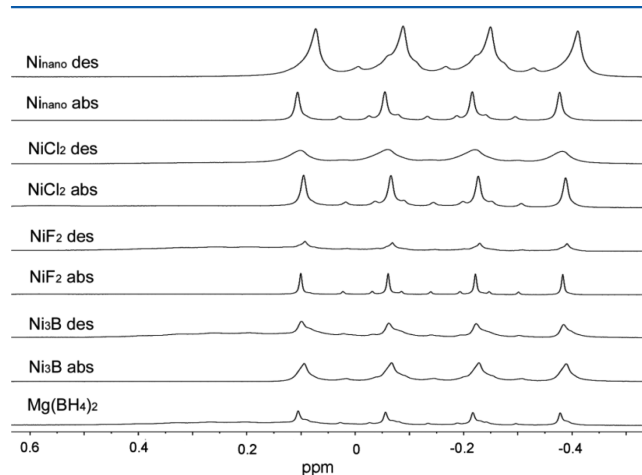


**Figure 5.** Stacked  $^1\text{H}$  NMR spectra of  $\text{Mg}(\text{BH}_4)_2$ – $\text{Ni}_{\text{add}}$  composites after desorption and absorption. All samples measured in  $\text{D}_2\text{O}$  solvent.

consisting of at least a quadruplet is observed in all spectra between 0.25 and –0.45 ppm after desorption, indicative of  $\text{Mg}(\text{BH}_4)_2$ . This suggests that total decomposition of  $\gamma$ - $\text{Mg}(\text{BH}_4)_2$  did not occur during hydrogen desorption, which was also evident by PXD analysis (Figure 1). Other broad features are observed, but their intensities are too weak for unambiguous assignment.

The decoupled  $^{11}\text{B}$  NMR spectra illustrated in Figure 6 provide a clear insight into the boron phases produced during hydrogen desorption–absorption of the  $\text{Mg}(\text{BH}_4)_2$ – $\text{Ni}_{\text{add}}$  composites. The resonance at –42 ppm in all spectra is attributed to  $\text{Mg}(\text{BH}_4)_2$  and confirms the incomplete decomposition of the initial  $\text{Mg}(\text{BH}_4)_2$ – $\text{Ni}_{\text{add}}$  composites.<sup>31,32</sup> All desorbed composite samples feature a resonance at –31 ppm, which is the most intense in the  $^{11}\text{B}$  NMR spectra apart from the  $\text{Mg}(\text{BH}_4)_2$ – $\text{Ni}_3\text{B}$  sample. After hydrogenation, this peak disappears completely, while the resonances at –42 ppm

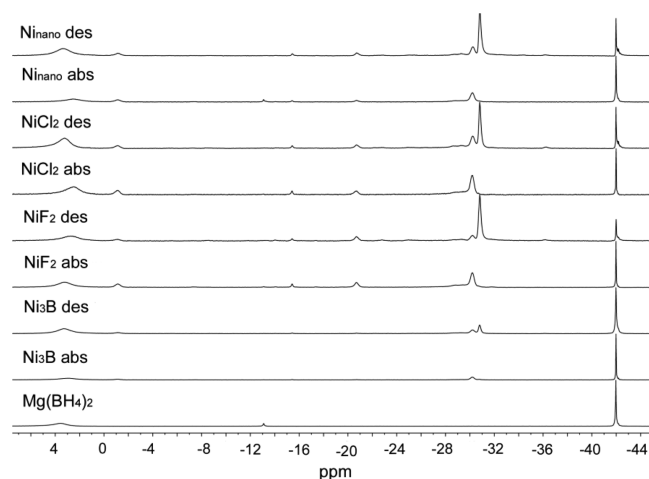


**Figure 6.** Stacked decoupled  $^{11}\text{B}$  NMR spectra of  $\text{Mg}(\text{BH}_4)_2\text{-Ni}_{\text{add}}$  composites after desorption and absorption. All samples measured in  $\text{D}_2\text{O}$  solvent.

( $[\text{BH}_4]^-$ ) and  $-30$  ppm, which are also observed after desorption, grow in intensity.

The peak at  $-31$  ppm can obviously be assigned to a reversible phase, which from general consensus can be attributed to  $[\text{B}_3\text{H}_8]^-$ .<sup>10,32</sup> The resonance at  $-30$  ppm can be assigned to  $[\text{B}_{10}\text{H}_{10}]^{2-}$ . Additional weak peaks are observed between  $-12$  and  $-24$  ppm, where the resonances for the  $[\text{B}_2\text{H}_6]^{2-}$ ,  $[\text{B}_5\text{H}_8]^-$ , and  $[\text{B}_{12}\text{H}_{12}]^{2-}$  anions are expected. This implies that the formation of the decomposition products  $[\text{B}_2\text{H}_6]^{2-}$ ,  $[\text{B}_5\text{H}_8]^-$ , and  $[\text{B}_{12}\text{H}_{12}]^{2-}$  is limited but not completely avoided even at a temperature below  $264^\circ\text{C}$ . Their concentration does not increase after hydrogenation, confirming their thermodynamic stability and their role in inhibiting reversibility of  $\text{Mg}(\text{BH}_4)_2$ . The fraction of  $[\text{B}_{10}\text{H}_{10}]^{2-}$  is significant already after desorption and increases after hydrogenation (Table 2). This might suggest that the Ni additives, which were expected to enhance the reversible hydrogenation of  $\text{Mg}(\text{BH}_4)_2$ , are also promoting the formation of  $[\text{B}_{10}\text{H}_{10}]^{2-}$ .

Another major resonance observed in the decoupled  $^{11}\text{B}$  NMR spectra is a broad feature at  $4$  ppm attributed to hydrolyzed borane derivatives, which are likely reaction products of boranes possessing open cage structures, such as *nido* or *arachno* boranes, and  $\text{D}_2\text{O}$  solvent.<sup>20–22</sup> Although the

measurements are conducted promptly after addition of the  $\text{D}_2\text{O}$  solvent, this reaction is unavoidably rapid, but the use of this solvent has been identified as the most efficient at dissolving the majority of the products associated with the reversible hydrogenation of  $\text{Mg}(\text{BH}_4)_2$ . On the other hand, IR analysis (see section 3.4) shows that the sample was possibly already contaminated with borates following the ball milling. Thus, the peak at  $4$  ppm can be at least partially due to these impurities. The amorphous and insoluble  $\text{Ni}_3\text{B}$  additives formed during desorption are not observed by liquid-state NMR spectroscopy.

The relative concentration of the boron-containing species measured by  $^{11}\text{B}$  NMR spectroscopy is summarized in Table 2. The data in the table suggest that the Ni additives promote both  $[\text{BH}_4]^-$  and  $[\text{B}_{10}\text{H}_{10}]^{2-}$  formation from  $[\text{B}_3\text{H}_8]^-$  during hydrogenation. The least relative concentration of the undesirable  $[\text{B}_{10}\text{H}_{10}]^{2-}$  is formed upon absorption in the presence of  $\text{Ni}_3\text{B}$ . There is an increase in relative concentration of  $[\text{BH}_4]^-$  in the  $\text{Ni}_{\text{nano}}$ -containing sample from  $0.25$  to  $0.94$  and an increase from  $0.18$  to  $0.34$  in the  $\text{NiF}_2$ -containing sample, but the most dramatic increase in integrated relative concentration is that of  $[\text{B}_{10}\text{H}_{10}]^{2-}$ .

**3.4. Infrared Study.** The IR spectra of the ball-milled, dehydrogenated, and rehydrogenated samples of  $\text{Mg}(\text{BH}_4)_2\text{-Ni}_{\text{add}}$  composites and pure  $\gamma\text{-Mg}(\text{BH}_4)_2$  are shown in Figure 7. For  $\gamma\text{-Mg}(\text{BH}_4)_2$  (Figure 7a) the IR data exhibit the internal vibrations of  $[\text{BH}_4]^-$  ions in the  $2900\text{--}600\text{ cm}^{-1}$  region. The B–H fundamental stretching modes are centered at  $2270\text{ cm}^{-1}$ , and the bending modes are located at ca.  $1420$  (broad),  $1260$ , and  $1130\text{ cm}^{-1}$ .<sup>33</sup> The peaks at  $2660$  and  $2400\text{ cm}^{-1}$  are assigned to the overtones and combinations of  $[\text{BH}_4]^-$  stretching and bending. According to Raman measurements and DFT calculations,  $\text{Mg}(\text{BH}_4)_2$  does not have normal modes of vibrations in the  $670\text{--}1120\text{ cm}^{-1}$  region.<sup>33</sup> Therefore, the peaks at  $913$  and  $706\text{ cm}^{-1}$  may be attributed to impurities, for example, boron oxides, due to small air contamination during sample preparation.

The spectrum of  $\text{Mg}(\text{BH}_4)_2$  is slightly altered after milling with the Ni-containing additives. The principal stretching and bending modes of  $[\text{BH}_4]^-$  are preserved, although their position is slightly shifted by  $2\text{--}5\text{ cm}^{-1}$ . For the as-milled  $\text{Mg}(\text{BH}_4)_2\text{-NiF}_2$  composite (Figure 7c) an additional peak at  $1194\text{ cm}^{-1}$  is clearly distinguishable. These changes may be induced by slight disorder in the  $[\text{BH}_4]^-$  structure and local environment.

**Table 2.** Integrated Relative Concentrations of Polyboranes in  $\text{Mg}(\text{BH}_4)_2\text{-Ni}_{\text{add}}$  ( $\text{Ni}_{\text{add}} = \text{Ni}_{\text{nano}}, \text{NiCl}_2, \text{NiF}_2, \text{Ni}_3\text{B}$ ) Composites in  $\text{D}_2\text{O}$  Solution after Hydrogen Desorption–Absorption and Pure  $\gamma\text{-Mg}(\text{BH}_4)_2$  Detected by  $^{11}\text{B}$  NMR Spectroscopy<sup>a</sup>

sample	borane species					
	$[\text{BH}_4]^-$	$[\text{B}_2\text{H}_6]^{2-}$	$[\text{B}_3\text{H}_8]^-$	$[\text{B}_5\text{H}_8]^-$	$[\text{B}_{10}\text{H}_{10}]^{2-}$	$[\text{B}_{12}\text{H}_{12}]^{2-}$
$\text{Ni}_{\text{nano}}$ des	0.25	0.09	1.00	0.00	0.35	0.03
$\text{Ni}_{\text{nano}}$ abs	0.94	0.11	0.00	0.09	1.00	0.04
$\text{NiCl}_2$ des	0.31	0.13	1.00	0.00	0.47	0.05
$\text{NiCl}_2$ abs	0.26	0.14	0.00	0.00	1.00	0.07
$\text{NiF}_2$ des	0.18	0.13	1.00	0.02	0.15	0.03
$\text{NiF}_2$ abs	0.34	0.27	0.06	0.01	1.00	0.08
$\text{Ni}_3\text{B}$ des	1.00	0.01	0.38	0.00	0.23	0.01
$\text{Ni}_3\text{B}$ abs	1.00	0.01	0.04	0.00	0.40	0.01
$\gamma\text{-Mg}(\text{BH}_4)_2$	1.00	0.00	0.00	0.08	0.00	0.00

<sup>a</sup>Chemical shifts:  $[\text{BH}_4]^-$ ,  $-42$  ppm;  $[\text{B}_2\text{H}_6]^{2-}$ ,  $-21$  ppm;  $[\text{B}_3\text{H}_8]^-$ ,  $-31$  ppm;  $[\text{B}_5\text{H}_8]^-$ ,  $-13$  ppm;  $[\text{B}_{10}\text{H}_{10}]^{2-}$ ,  $-30$  ppm;  $[\text{B}_{12}\text{H}_{12}]^{2-}$ ,  $-15$  ppm. The strongest peak is set to 1.00.

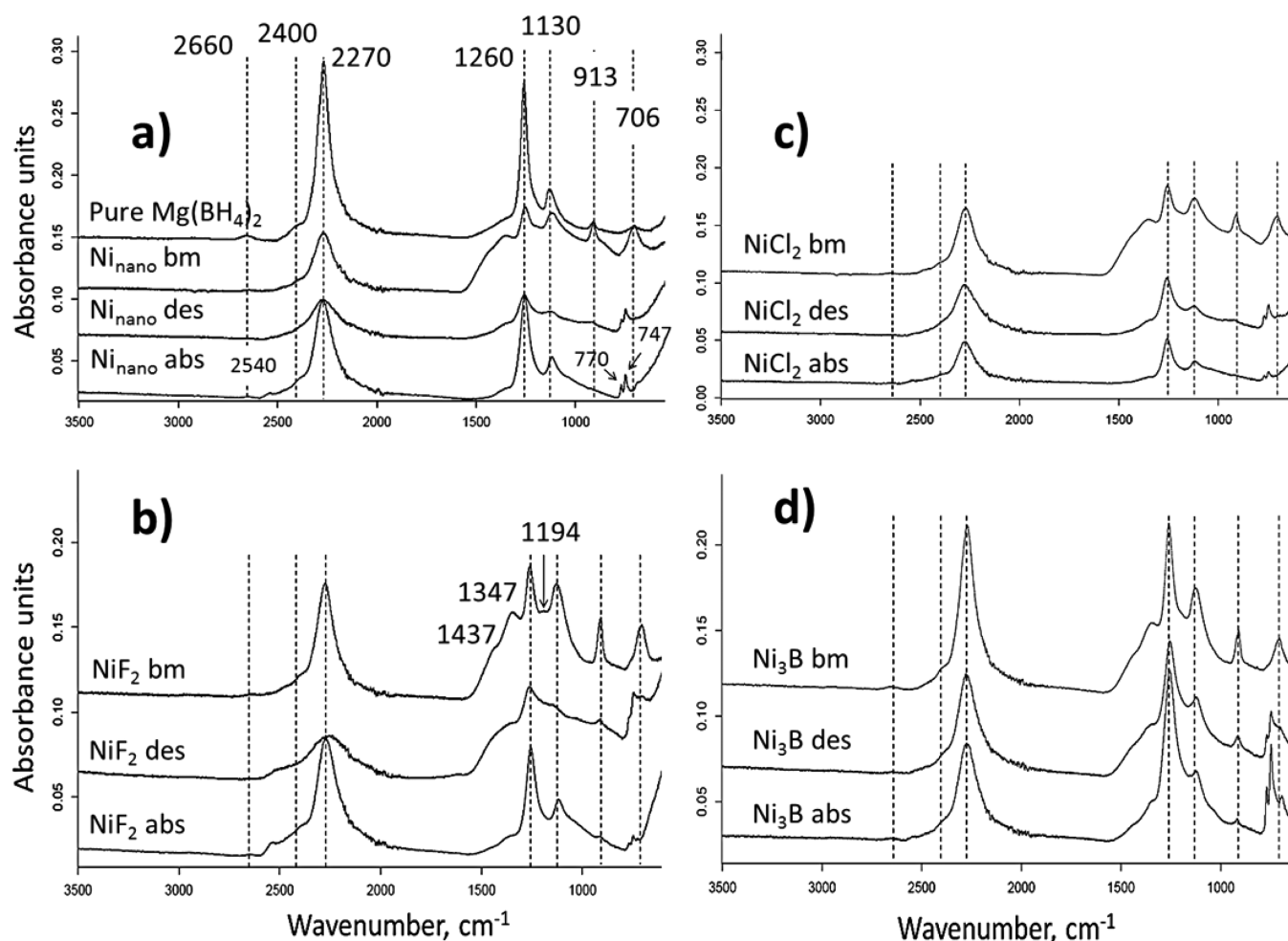


**Figure 7.** IR spectra of  $\text{Mg}(\text{BH}_4)_2\text{-Ni}_{\text{add}}$  ( $\text{Ni}_{\text{add}}$  = (a)  $\text{Ni}_{\text{nano}}$ , (b)  $\text{NiF}_2$ , (c)  $\text{NiCl}_2$ , (d)  $\text{Ni}_3\text{B}$ ) composites and starting  $\gamma\text{-Mg}(\text{BH}_4)_2$ . The peaks present in  $\gamma\text{-Mg}(\text{BH}_4)_2$  are indicated with dashed lines. The spectra are offset in the vertical direction for better representation and comparison.

The spectra of the samples after desorption exhibit an overall decrease in the intensities of the B–H stretching and bending bands, which is indicative of a decreased amount of  $[\text{BH}_4]^-$  groups compared to the spectra of ball-milled compounds. The fingerprint spectrum of  $\text{Mg}(\text{BH}_4)_2$ , however, is still recognizable in all spectra after desorption. This is consistent with the PXD and NMR results, which identifies a small amount of  $[\text{BH}_4]^-$  in all the samples after desorption. Additionally, for the  $\text{NiF}_2$ -milled sample, a weak absorption peak with a distinct maximum at ca.  $2540\text{ cm}^{-1}$  appears. This is the region (between  $2550$  and  $2400\text{ cm}^{-1}$ ) where the B–H stretching of the *closo* boranes  $[\text{B}_{12}\text{H}_{12}]^{2-}$  and  $[\text{B}_{10}\text{H}_{10}]^{2-}$  is expected as strong bands centered at  $2485$  and  $2467\text{ cm}^{-1}$ , respectively.<sup>34</sup>  $[\text{B}_{12}\text{H}_{12}]^{2-}$  has additional IR-active vibrations at  $1070\text{ cm}^{-1}$  (H–B–B bending, medium in intensity) and at  $720\text{ cm}^{-1}$  (B–B stretching, medium);  $[\text{B}_{10}\text{H}_{10}]^{2-}$  also absorbs at  $1030\text{ cm}^{-1}$  (H–B–B bending, medium in intensity) and  $720\text{ cm}^{-1}$  (B–B stretching, medium).<sup>34</sup> The latter peak is considered to be a fingerprint of *closo* boranes.<sup>34</sup> On the basis of the very weak intensity of the B–H stretching peaks, it is possible that the B–B–H bending and B–B stretching is obscured in the  $1100\text{--}700\text{ cm}^{-1}$  region. New small peaks at  $770$  and  $747\text{ cm}^{-1}$ , where B–B–H bending is expected, appear in the spectra of all samples after desorption, but their origin is unclear.

In the spectra of  $\text{Ni}_{\text{nano}}$ - and  $\text{NiF}_2$ -containing samples after absorption (Figure 7a,b), the intensity of the bands due to

$[\text{BH}_4]^-$  and  $[\text{B}_n\text{H}_n]^{2-}$  increases. The intensity of the vibrations due to  $[\text{BH}_4]^-$  remains almost unchanged after hydrogen absorption in the  $\text{NiCl}_2$  and  $\text{Ni}_3\text{B}$  composites. These findings are consistent with the changes in the relative concentrations of these moieties identified by NMR. Finally, it can be noted that the strongest peaks due to  $[\text{B}_n\text{H}_n]^{2-}$  bending are present in the  $\text{NiF}_2$ -containing composite, and the weakest in the one with  $\text{Ni}_3\text{B}$ . These samples were treated at the highest and the lowest temperature, respectively. On the other hand, it is important to point out that the relative intensities of the IR vibrations of  $[\text{BH}_4]^-$  and  $[\text{B}_n\text{H}_n]^{2-}$  do not necessarily reflect the relative concentration of these species in the mixture. The intensities of the IR peaks in attenuated total reflection measurements, used in this work, strongly depend on the refractive indexes of the materials. Comparing the intensity ratios of different samples, however, is reasonable.

The  $^{11}\text{B}$ -NMR results indicate  $[\text{B}_3\text{H}_8]^-$  as the main phase of the dehydrogenated samples and the significant decrease in its amount upon reabsorption. However, the IR data do not unambiguously confirm the presence of the  $[\text{B}_3\text{H}_8]^-$  in the dehydrogenated samples. An important distinguishable IR feature of these types of compounds is the B–H stretching of the B–H–B bridged hydrogen found as low as  $2150\text{--}2000\text{ cm}^{-1}$ . This region is almost unaffected in the samples upon cycling (Figure 7, desorption and absorption).



## 4. CONCLUSIONS

$\gamma$ -Mg(BH<sub>4</sub>)<sub>2</sub> was milled with a variety of Ni-based additives, 2 mol % Ni<sub>nanor</sub>, NiCl<sub>2</sub>, NiF<sub>2</sub>, and Ni<sub>3</sub>B, to study their effect on the reversible hydrogenation of the borohydride. Powders were sampled after milling and hydrogen desorption–absorption in order to monitor the structural changes in the hydrogen-containing phases with PXD, XAS, NMR, and IR spectroscopies. The key conclusions are as follows:

- (1) Chemical reactions between the Ni-based additives and  $\gamma$ -Mg(BH<sub>4</sub>)<sub>2</sub> do not take place during ball milling, although the crystallinity of the borohydride decreases.
- (2) During hydrogen desorption of Mg(BH<sub>4</sub>)<sub>2</sub>–NiCl<sub>2</sub> at 258 °C and Mg(BH<sub>4</sub>)<sub>2</sub>–NiF<sub>2</sub> at 264 °C, the used additives react with the intermediate boranes to form new compounds with amorphous Ni<sub>3</sub>B-like structure.
- (3) Hydrogen desorption results in the formation of a reversible phase which was identified by <sup>11</sup>B NMR as Mg(B<sub>3</sub>H<sub>8</sub>)<sub>2</sub>. However, IR could not confirm the presence of the B–H–B bridged bonds, characteristic of Mg(B<sub>3</sub>H<sub>8</sub>)<sub>2</sub>.
- (4) Upon rehydrogenation at pressures between 100 and 150 bar, crystalline  $\beta$ -Mg(BH<sub>4</sub>)<sub>2</sub> is formed at the expenses of the reversible phase. During hydrogenation, all of the Ni additives react to form the thermodynamically stable Ni<sub>3</sub>B.

These results, compared with those of previous studies,<sup>10</sup> suggest that the incorporation of Ni additives into Mg(BH<sub>4</sub>)<sub>2</sub> enhances the kinetics of hydrogen desorption from Mg(BH<sub>4</sub>)<sub>2</sub>. For instance, in the Mg(BH<sub>4</sub>)<sub>2</sub>–Ni<sub>3</sub>B sample, we observe the desorption of 2.7 wt % H<sub>2</sub> in 15 h at 220 °C. This desorption time is significantly shorter than 5 weeks (more than 800 h) required for pure Mg(BH<sub>4</sub>)<sub>2</sub> at 200 °C.<sup>10</sup> At the same time, interplay of low desorption temperatures and Ni additives possibly limits the formation of higher boranes, which are believed to hinder the reversibility of Mg(BH<sub>4</sub>)<sub>2</sub>. Additional characterization techniques, e.g., <sup>11</sup>B solid-state NMR, coupled with advanced modeling methods are required to unambiguously identify the reversible phase found in this work.

## ■ ASSOCIATED CONTENT

### Supporting Information

Normalized X-ray absorption spectra of Mg(BH<sub>4</sub>)<sub>2</sub>–Ni<sub>add</sub> composites in the as-milled state together with corresponding Ni additive as reference. This material is available free of charge via the Internet at <http://pubs.acs.org>.

## ■ AUTHOR INFORMATION

### Corresponding Author

\*E-mail: [bjorn.hauback@ife.no](mailto:bjorn.hauback@ife.no). Tel.: +47 97 40 88 44.

### Notes

The authors declare no competing financial interest.

## ■ ACKNOWLEDGMENTS

The help from Dr. C. M. Frommen, Dr. J. E. Olsen (preparation of Ni<sub>3</sub>B starting material), and Mr. J. Martens (production of the XAFS sample holder) at IFE is gratefully acknowledged. Dr. S. Carlson and Dr. K. Sigfridsson are thanked for assistance and guidance at beamline I811 in Max-Lab, Sweden. This work was supported by the Norwegian Research Council within the NANOMAT (Project 182040/S10) and FRIENERGI programs (Project 197756/F20), and by

the European Fuel Cells and Hydrogen Joint Undertaking (<http://www.fch-ju.eu>) under collaborative project “BOR4-STORE” (Grant Agreement: N° 303428).

## ■ REFERENCES

- (1) Orimo, S.; Nakamori, Y.; Eliseo, J. R.; Züttel, A.; Jensen, C. M. Complex Hydrides for Hydrogen Storage. *Chem. Rev. (Washington, DC, U.S.)* **2007**, *107*, 4111–4132.
- (2) Riktor, M. D.; Sørby, M. H.; Fichtner, M.; Chłopek, K.; Buchter, F.; Züttel, A.; Hauback, B. C. In Situ Synchrotron Diffraction Studies of Phase Transitions and Thermal Decomposition of Mg(BH<sub>4</sub>)<sub>2</sub> and Ca(BH<sub>4</sub>)<sub>2</sub>. *J. Mater. Chem.* **2007**, *17*, 4939–4942.
- (3) Chłopek, K.; Frommen, C.; Leon, A.; Zabara, O.; Fichtner, M. Synthesis and Properties of Magnesium Tetrahydroborate, Mg(BH<sub>4</sub>)<sub>2</sub>. *J. Mater. Chem.* **2007**, *17*, 1396–13503.
- (4) Li, H. W.; Kikuchi, K.; Nakamori, Y.; Ohba, N.; Miwa, K.; Towata, S.; Orimo, S. Dehydrogenation and Rehydrogenation Processes of Well-Crystallized Mg(BH<sub>4</sub>)<sub>2</sub> Accompanying with Formation of Intermediate Compounds. *Acta Mater.* **2008**, *56*, 1342–1347.
- (5) Soloveychik, G.; Gao, Y.; Rijssenbeek, J.; Andrus, M.; Kniajanski, S.; Bowman, R. C.; Hwang, S. J.; Zhao, Ch. Magnesium Borohydride as a Hydrogen Storage Material: Properties and Dehydrogenation Pathway of Unsolvated Mg(BH<sub>4</sub>)<sub>2</sub>. *J. Hydrogen Energy* **2009**, *34*, 916–928.
- (6) Rönnebro, E. Development of Group II Borohydrides as Hydrogen Storage Materials. *Curr. Opin. Solid State Mater. Sci.* **2011**, *15*, 44–51.
- (7) Ozoliņš, V.; Majzoub, E. H.; Wolverton, C. First-Principles Prediction of Thermodynamically Reversible Hydrogen Storage Reactions in the Li-Mg-Ca-B-H system. *J. Am. Chem. Soc.* **2009**, *131*, 230–237.
- (8) Hwang, S.; Bowman, R. C.; Reiter, J. J. W.; Rijssenbeek, J.; Soloveichik, G. L.; Zhao, J.; Kabbour, H.; Ahn, C. C. NMR Confirmation for Formation of [B<sub>12</sub>H<sub>12</sub>]<sup>2-</sup> Complexes during Hydrogen Desorption from Metal Borohydrides. *J. Phys. Chem. C* **2008**, *112*, 3164–3169.
- (9) Li, H. W.; Miwa, K.; Ohba, N.; Fujita, T.; Sato, T.; Yan, Y.; Towata, S.; Chen, M. W.; Orimo, S. Formation of an Intermediate Compound with a B<sub>12</sub>H<sub>12</sub> Cluster: Experimental and Theoretical Studies on Magnesium Borohydride Mg(BH<sub>4</sub>)<sub>2</sub>. *Nanotechnology* **2009**, *20*, 204013–204020.
- (10) Chong, M.; Karkamkar, A.; Autrey, T.; Orimo, S.; Jalilati, S.; Jensen, C. M. Reversible Dehydrogenation of Magnesium Borohydride to Magnesium Triborane in the Solid State under Moderate Conditions. *Chem. Commun. (Cambridge, U.K.)* **2011**, *47*, 1330–1332.
- (11) Barkhordarian, G.; Klassen, T.; Borman, R. Catalytic Mechanism of Transition-Metal Compounds on Mg Hydrogen Sorption Reaction. *J. Phys. Chem. B* **2006**, *110*, 11020–11024.
- (12) Ignatov, A. Yu.; Graetz, J.; Chaudhuri, S.; Salguero, T. T.; Vajo, J. J.; Meyer, F. E.; Pinkerton, M. S.; Tyson, T. A. Spatial Configurations of Ti- and Ni- Species Catalyzing Complex Metal Hydrides: X-Ray Absorption Studies and First-Principles DFT and MD Calculations. *AIP Conf. Proc.* **2007**, *882*, 642–644.
- (13) Graetz, J.; Chaudhuri, S.; Salguero, T. T.; Vajo, J. J.; Meyer, M. S.; Pinkerton, F. E. Local Bonding and Atomic Environments in Ni-catalyzed Complex Hydrides. *Nanotechnology* **2009**, *20*, 204007–204015.
- (14) Jiang, Z.; Yang, H.; Wei, Z.; Xie, Z.; Zhong, W.; Wie, S. Catalytic Properties and Structures of Nano-Amorphous Ni–B Alloys Affected by Annealing Temperatures. *Appl. Catal., A* **2005**, *279*, 165–171.
- (15) Humphries, T. D.; Kalantzopoulos, G. N.; Llamas-Jansa, I.; Olsen, J. E.; Hauback, B. C. Reversible Hydrogenation Studies of NaBH<sub>4</sub> Milled with Ni-Containing Additives. *J. Phys. Chem. C* **2013**, *117*, 6060–6065.
- (16) Kapfenberger, C.; Hofmann, K.; Albert, B. Room-Temperature Synthesis of Metal Borides. *Solid State Sci.* **2003**, *5*, 925–930.

- (17) Brinks, H. W.; Fossdal, A.; Bowman, R. C., Jr.; Hauback, B. C. Pressure–Composition Isotherms of  $\text{TbNiAlH}_x$ . *J. Alloys Compd.* **2006**, *417*, 92–95.
- (18) Carlson, S.; Clausen, M.; Gridneva, L.; Sommarin, B.; Svensson, C. XAFS Experiments at Beamline I811, MAX-Lab Synchrotron Source, Sweden. *J. Synchrotron Radiat.* **2006**, *13*, 359–364.
- (19) Ravel, B.; Newville, M. ATHENA, ARTEMIS, HEPHAESTUS: Data Analysis for X-Ray Absorption Spectroscopy Using IFEFFIT. *J. Synchrotron Radiat.* **2005**, *12*, 537–541.
- (20) Aftandilian, V. D.; Miller, H. C.; Muetterties, E. L.; Parshall, G. W. Chemistry of Boranes. V. First Example of a  $\text{B}_{11}$  Hydride, the  $\text{B}_{11}\text{H}_{14}^-$  Anion. *Inorg. Chem.* **1962**, *1*, 734–737.
- (21) Muetterties, E. L.; Balthis, J. H.; Miller, H. C.; Chia, Y. T.; Knoth, W. H. Chemistry of Boranes. VIII. Salts and Acids of  $\text{B}_{10}\text{H}_{10}^{-2}$  and  $\text{B}_{12}\text{H}_{12}^{-2}$ . *Inorg. Chem.* **1964**, *3*, 444–451.
- (22) Tiritiris, I.; Schleid, T. Dodekahydro-*closo*-Dodekaborate  $\text{M}_2[\text{B}_{12}\text{H}_{12}]$  der Schweren Alkalimetalle ( $\text{M}^+ = \text{K}^+, \text{Rb}^+, \text{NH}_4^+, \text{Cs}^+$ ) und Ihre Formalen Iodid-Addukte  $\text{M}_3\text{I}[\text{B}_{12}\text{H}_{12}]$  ( $\equiv \text{MI} \cdot \text{M}_2[\text{B}_{12}\text{H}_{12}]$ ). *Z. Anorg. Allg. Chem.* **2003**, *629*, 1390–1402.
- (23) Li, H. W.; Kikuchi, K.; Nakamori, Y.; Miwa, K.; Towata, S.; Orimo, S. Effects of Ball Milling and Additives on Dehydriding Behaviors of Well-Crystallized  $\text{Mg}(\text{BH}_4)_2$ . *Scr. Mater.* **2007**, *57*, 679–682.
- (24) Filinchuk, Y.; Richter, B.; Jensen, T. R.; Dmitriev, V.; Chernyshov, D.; Hagemann, H. Porous and Dense  $\text{Mg}(\text{BH}_4)_2$  Frameworks: Synthesis, Stability and Reversible Absorption of Guest Species. *Angew. Chem., Int. Ed.* **2011**, *50*, 11162–11166.
- (25) Paskevicius, M.; Pitt, M. P.; Webb, C. J.; Sheppard, D. A.; Filso, U.; Gray, E. M.; Buckley, C. E. In-Situ X-ray Diffraction Study of  $\gamma$ - $\text{Mg}(\text{BH}_4)_2$  Decomposition. *J. Phys. Chem. C* **2012**, *116*, 15231–15240.
- (26) Wei, S.; Oyanagi, H.; Li, Z.; Zhang, X.; Liu, W.; Yin, S.; Wang, X. X-ray-Absorption Fine Structure Study on Devitrification of Ultrafine Amorphous Ni-B Alloys. *Phys. Rev. B* **2001**, *63*, 224201–224206.
- (27) Wei, Z.; Li, Z.; Jiang, Z.; Ye, J.; Zhong, W.; Song, J.; Wei, S. In-Situ XAFS Study on Structures and Devitrifications of Ni–B Nano-Amorphous Alloys. *J. Alloys Compd.* **2008**, *460*, 553–558.
- (28) Wei, S.; Li, Z.; Yin, S.; Zhang, X.; Liu, W.; Wang, X. Annealed Crystallization of Ultrafine Amorphous NiB Alloy Studied by XAFS. *J. Synchrotron Radiat.* **2001**, *8*, 566–568.
- (29) Wei, Z.; Jiang, Z.; Ye, J.; Zhong, W.; Song, J.; Wie, S. In-Situ XAFS Investigation of the Crystallization Mechanism of Ni-B Nano-Amorphous Alloy. *AIP Conf. Proc.* **2007**, *882*, 771–773.
- (30) Kapfenberger, C. *Synthese und Charakterisierung von nano-skalierten Nickelboriden*; PhD Thesis, Hamburg University Press: Hamburg, Germany, 2005.
- (31) Choi, Y. J.; Lu, J.; Sohn, H. Y.; Fang, Z. Z.; Kim, C.; Bowman, R. C., Jr.; Hwang, S. J. Reaction Mechanisms in the  $\text{Li}_3\text{AlH}_6/\text{LiBH}_4$  and  $\text{Al}/\text{LiBH}_4$  Systems for Reversible Hydrogen Storage. Part 2: Solid-State NMR Studies. *J. Phys. Chem. C* **2011**, *115*, 6048–6056.
- (32) Wrackmeyer, B. Indirect Nuclear Spin-Spin Coupling Constants  $^nJ(^{11}\text{B}, ^1\text{H})$  and  $^nJ(^{11}\text{B}, ^{11}\text{B})$  in Some Boron Hydrides – Density Functional Theory (DFT) Calculations. *Z. Naturforsch., B: Chem. Sci.* **2004**, *59b*, 1192–1199.
- (33) Giannasi, A.; Colognesi, D.; Ulivi, L.; Zoppi, M.; Ramirez-Cuesta, A. J.; Bardaji, E. G.; Roehm, E.; Fichtner, M. High Resolution Raman and Neutron Investigation of  $\text{Mg}(\text{BH}_4)_2$  in an Extensive Temperature Range. *J. Phys. Chem. A* **2010**, *114*, 2788–2793.
- (34) Leites, L. A. Vibrational Spectroscopy of Carboranes and Parent Boranes and its Capabilities in Carborane Chemistry. *Chem. Rev. (Washington, DC, U.S.)* **1992**, *92*, 279–323.